PERSPECTIVE
https://doi.org/10.1038/s41929-021-00683-1

nature catalysis

Check for updates

Uniting biological and chemical strategies for selective CO_2 reduction

Hannah S. Shafaat [1]✉ and Jenny Y. Yang [2]✉

The electrochemical reduction of CO_2 into useful fuels and chemical feedstocks offers great promise for conversion to a carbon-neutral economy. However, challenges in product selectivity continue to limit the practical application of electrocatalytic systems. In this Perspective, we outline the thermodynamic and kinetic factors for the design of improved catalysts for CO_2 fixation and carbon–carbon bond formation, and draw parallels between synthetic systems and natural enzymes that perform analogous transformations. By identifying the primary features that underpin the highly efficient CO_2 conversion reactions seen in nature, synthetic catalysts can be constructed to take advantage of similar chemical principles. Given the demonstrated prior success of bio-inspired molecular design, increased and dynamic interactions between the chemical, biological and materials science fields will advance catalyst development in a synergistic fashion.

There is an ecological imperative to reduce society's reliance on fossil fuels[1]. To accomplish this, several technological advancements are required for a carbon-neutral and sustainable future. A key component is to advance energy storage technologies to flex intermittent renewable sources of energy into an on-demand framework. Although many solutions currently exist—from batteries to pumped hydroelectricity—chemical fuels continue to be one of the highest density forms of energy storage[2]. Among the different approaches to chemical energy storage, the reduction of carbon dioxide (CO_2) to give carbon-based liquid fuels is one of the most popular approaches. The feedstock (CO_2) is abundant and the resulting fuels easily integrate into our current carbon-fuel-based energy infrastructure. CO_2 capture and concentration, particularly from air, is still a challenge, but it is also an active area of research[3]. Decreasing our reliance on fossil fuels for energy will concurrently curtail our primary sources of carbon-based feedstock chemicals (for example, olefins) for materials synthesis. Therefore, valorizing CO_2 into synthetic precursors or direct conversion into materials is also a key goal as we move towards carbon neutrality. An analysis on the economic value of various CO_2 reduction products that can be used as fuels or synthetic precursors was recently published[4].

CO_2 can be reduced to multiple products through hydrogenation or electrochemical reduction. Carbon-neutral hydrogenation can be achieved using 'green hydrogen'[5], or H_2 derived from the electrolysis of water using renewable electricity. The focus of this perspective will be on the direct electrochemical reduction of CO_2. Electrochemical reduction presents several advantages over hydrogenation. As the protons used for reduction derive directly from solution, there is no need to handle flammable H_2 gas. Additionally, hydrogenation reactions frequently require high temperatures and pressures, which are not typically required for electrolytic methods.

However, product selectivity is a greater challenge in electrochemical reduction compared with that in hydrogenation. In addition to multiple possible CO_2 reduction products, direct H^+ reduction to H_2 is often a competitive reaction, which diverts electron equivalents to a non-carbon-based product. Parasitic H_2 evolution is currently one of the biggest impediments to selective CO_2 reduction. This Perspective focuses on thermodynamic and kinetic considerations for selective CO_2 reduction, and draws parallels with our current understanding of natural enzymes that perform analogous reactions to those of synthetic systems. Biological CO_2 fixation requires many of the same steps as the effective anthropogenic synthesis of liquid fuels: long-range electron transfer, capture of gaseous reactants, sequential (cascade) catalysis, substrate channelling, dynamic secondary sphere interactions, conformational changes, ordered binding and reversibility. Although there are notable successful examples of installing some of these features into synthetic systems[6,7], it is likely that incorporating more of these principles will be necessary to effect analogous reactivity. Nature has optimized the conversion of CO_2 into the two-electron-reduced products, formate and carbon monoxide (CO), using specialized metalloenzymes. Furthermore, selective integration of CO_2, CO and formate into complex biomolecules through the formation of new C–C bonds represents the paradigm that synthetic and bio-inspired chemists and catalysis scientists seek to replicate.

Thermodynamic considerations

Figure 1a provides the standard potentials for direct proton reduction as well as for major CO_2 reduction products. We note that the high potentials required for the one-electron reduction of CO_2 and H^+ to form the radicals $CO_2^{\bullet-}$ and $H^\bullet$ (−1.90 and −2.31 V versus the standard hydrogen electrode (SHE), respectively) generally compel such substrates to be activated through the binding or interaction with a catalyst[8]. Among the major products for the $2e^-$ reduction of CO_2, only three are more challenging in terms of standard potential than the direct proton reduction to H_2: CO, formic acid (HCOOH) and oxalic acid ($(COOH)_2$). CO_2 reduction to CO and $2H^+$ reduction to H_2 are both $2H^+$, $2e^-$ reactions. Therefore, their relative thermodynamic potentials change as a function of pH with the same slope (59 mV $(\log[H^+])^{-1}$) as given by the Nernst equation. However, HCOOH and $(COOH)_2$ represent unique cases as they are relatively acidic. For HCOOH, under conditions in which it is deprotonated (pH > 3.75 in H_2O, pK_a > 20.9 in CH_3CN), CO_2 reduction produces formate, which is a $2e^-$, $1H^+$ process. Thus, instead of the thermodynamic potential decreasing by 59 mV $(\log[H^+])^{-1}$, it will decrease by 29.5 mV $(\log[H^+])^{-1}$, or have

[1]Department of Chemistry and Biochemistry, The Ohio State University, Columbus, OH, USA. [2]Department of Chemistry, University of California, Irvine, CA, USA. ✉e-mail: Shafaat.1@osu.edu; j.yang@uci.edu

a

Half reactions	Potential (V) versus SHE
$H^+ + e^- \rightarrow H^\bullet$	–2.31
$CO_2 + e^- \rightarrow CO_2^{\bullet-}$	–1.90
$2H^+ + 2e^- \rightarrow H_2$ (g)	0.0
CO_2 (g) + $2H^+$ + $2e^- \rightarrow$ HCOOH (l)	–0.12
CO_2 (g) + $2H^+$ + $2e^- \rightarrow$ CO (g) + H_2O (l)	–0.10
$2CO_2$ (g) + $2H^+$ + $2e^- \rightarrow$ $(COOH)_2$ (l)	–0.47
CO_2 (g) + $6H^+$ + $2e^- \rightarrow$ CH_3OH (l) + H_2O (l)	–0.03
CO_2 (g) + $8H^+$ + $8e^- \rightarrow$ CH_4 (g) + $2H_2O$ (l)	0.17
CO_2 (g) + $8H^+$ + $8e^- \rightarrow$ CH_3COOH (l) + $2H_2O$ (l)	0.11
$2CO_2$ (g) + $12H^+$ + $12e^- \rightarrow$ C_2H_4 (g) + $2H_2O$ (l)	0.14
$2CO_2$ (g) + $12H^+$ + $12e^- \rightarrow$ CH_3CH_2OH (l) + $3H_2O$ (l)	0.09

b

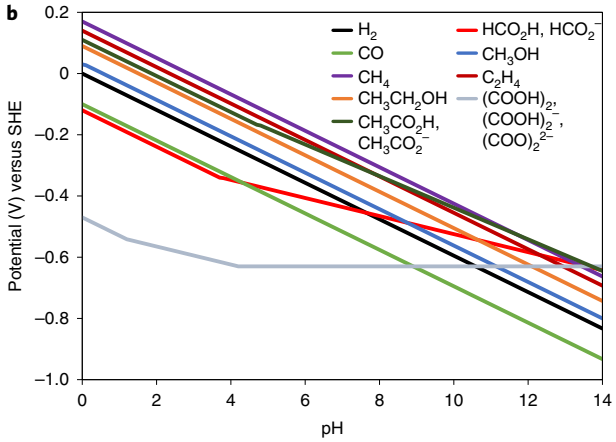

Fig. 1 | Thermodynamic values associated with H^+ and CO_2 reduction. **a**, Table of reduction potentials for H^+ and CO_2 reduction to a variety of products under standard conditions. **b**, Corresponding Pourbaix diagram, which depicts how the potentials change with respect to pH for $2e^-$ and greater reduction reactions.

a shallower slope in the Pourbaix diagram (Fig. 1b). As a result, the thermodynamic potential for CO_2 to give HCO_2^- becomes more positive than the $2H^+/H_2$ couple at pH 8.1 in aqueous solutions ($pK_a > 25.9$ in CH_3CN and $pK_a > 13.6$ in dimethyl sulfoxide)[9]. This type of behaviour is also observed for other CO_2 reduction products with acidic protons, such as $(COOH)_2$; above pH 10.6, CO_2 reduction to the dianion oxalate ($(COO)_2^{2-}$) is more favourable than direct H^+ reduction. The same phenomenon occurs with acetic acid (CH_3COOH) and methanol (CH_3OH), although CH_3OH is considerably less acidic. For CH_3COOH, the standard potential is already positive of the $2H^+/H_2$ couple. Under conditions in which CH_3COOH is deprotonated, the acetate will increasingly be the thermodynamically favoured product (over H_2 evolution) with decreasing proton activity ($\log[H^+]$).

As demonstrated by Fig. 1, the free energy of CO_2 reduction to most products is more favourable than the direct H^+ reduction to H_2. In cases for which the synthetic catalysts are optimized to operate at a minimal overpotential, selectivity can be achieved because H_2 evolution is endergonic[7]. However, applying even modest overpotentials will result in exergonic H_2 evolution. Additionally, the small potential range for most carbon-based products further complicates selectivity towards a single product.

Kinetic considerations

Selectivity between various CO_2 reduction products and the direct reduction of H^+ to H_2 is ultimately determined by the reaction sequence of protons and electrons (and/or their coupled transfer) and CO_2 with the catalyst. Bio-inspired strategies to control the CO_2 versus H^+ transfer to active sites focuses on the electronic structure of the active site and the outer coordination sphere effects. Each of these strategies is discussed with respect to their biological context, and how they can be reproduced in synthetic systems (Fig. 2).

CO_2-reduction catalysis for most products (with the exception of formate) is initiated when CO_2 is activated by the reduced catalyst. As CO_2 is relatively inert, activation at a single site often requires an electron-rich (nucleophilic), highly reduced metal centre. The negative potential required, in turn, increases the overall overpotential. Highly reduced metal centres also tend to be more basic, and are therefore prone to protonation, which often leads to H_2 evolution[10]. However, there are a few catalyst design strategies towards selectively activating CO_2 over direct protonation.

Several of these strategies are inspired by the carbon monoxide dehydrogenase (CODH) enzymes. The electrocatalytic activity of NiFe–CODH, a CODH of the anaerobic bacterium *Carboxydothermus hydrogenoformans*, displays reversible electrocatalytic conversion of CO_2 to give CO with high rates at the thermodynamic potential (no overpotential) or at –520 mV versus SHE at pH 7 (ref. [11]). The catalytic site of NiFe–CODH features a unique, site-differentiated [4Fe–4S–Ni] centre, with a reduction potential that is well-matched to the CO_2/CO couple (Fig. 2a)[6]. The electronic communication across the non-canonical heterometallic cluster delocalizes the excess electrons across the entire fragment[12], which promotes facile charge migration through the cluster on CO_2 binding while lowering the nucleophilicity (Brönsted basicity) of any individual metal centre, which reduces the propensity for protonation and subsequent H_2 evolution[13].

Another approach used by CODH to control the reactivity for CO_2 versus H^+ is electronic control. Prior to CO_2 binding, the formally Ni^0 centre has a distorted T-shaped geometry[13,14]. The π-donating character of the sulfide and thiolate ligands in the fully reduced cluster should enforce π symmetry on the frontier molecular orbitals, which promotes the activation of CO_2 predominantly through π back donation rather than through the σ interaction, which could also enable proton binding and hydride formation[15,16]. Indeed, although Ni^{II}–H formation was invoked in the past as an intermediate in CO_2 activation[17], such a species was largely ruled out on the basis of careful reactivity and electronic structure studies[13,18]. In a synthetic analogue, the symmetry of the frontier orbitals was invoked as the basis for the high selectivity for CO_2 to CO by the well-studied molecular electrocatalyst $Re(bpy)(CO)_3Cl$ (bpy, bipyridine) (Fig. 2b)[19]. Accessible oxidation states can also influence the reactivity of CO_2 versus H^+ at a reduced centre. CO_2 activation can involve either a formal $1e^-$ oxidation of the metal to form a metal-bound carboxylate radical anion, which is usually stabilized relative to free $CO_2^{\bullet-}$, or a $2e^-$ oxidation to form the fully reduced anionic carboxylate ligand. However, H^+ binding to form a metal hydride formally oxidizes the metal by two electrons. Thus, controlling the accessibility of the $1e^-$ versus $2e^-$ redox couples of the catalyst can favour reactivity towards CO_2.

Another bio-inspired method to facilitate selective CO_2 activation to a specific product is cooperativity. The X-ray crystallographic structure of NiFe–CODH under reducing conditions in the presence of CO_2 suggests a cooperative binding by Ni and Fe, assisted by hydrogen bonding to two basic amino acids, a lysine and a histidine, as shown in Fig. 2c[11]. Electrophilic activation of CO_2 occurs through the direct binding of carbon to the electron-rich formal Ni^0 site, stabilized by bridging to the adjacent Fe_u^{2+} centre through oxygen ligation. Thus, the active site capitalizes on a secondary metal interaction to effectively chelate CO_2 in an asymmetric fashion, which promotes a selective protonation of the Fe-bound oxygen atom and C–O bond cleavage to form CO. The accompanying electronic assistance from the supporting iron–sulfur cluster enables a multielectron reduction without the accumulation of a substantial charge or spin density at any one particular site[13,20]. These cooperative interactions stabilize the carboxylate intermediate, which results in CO_2 activation at a mild potential.

The advantage of cooperative CO_2 activation over single-site catalysts can be viewed through a Sabatier analysis[21]. For monometallic

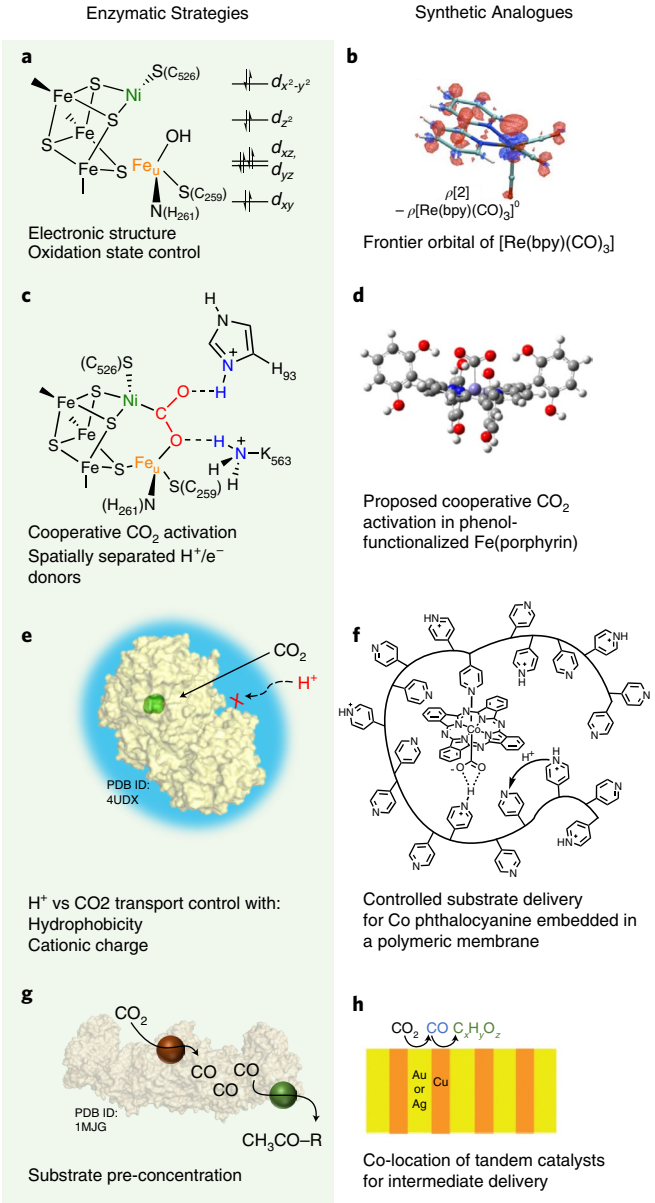

Fig. 2 | Enzymatic strategies for selective CO_2 reduction and a selection of synthetic analogues. a, Active site structure and putative approximate Ni *d*-orbital ordering for *C. hydrogenoformans II* NiFe-CODH. **b**, Calculated frontier orbital of synthetic catalyst [Re(bpy)$(CO)_3$]. **c**, Structure of the proposed CO_2-bound intermediate in *C. hydrogenoformans II* NiFe-CODH illustrating the interactions with secondary coordination sphere residues. **d**, Proposed CO_2-bound intermediate in a phenol-functionalized Fe(porphyrin) catalyst. **e**, Depiction of outer-sphere control over H^+ and CO_2 transport in *C. hydrogenoformans II* NiFe-CODH with hydrophobicity and cationic charge. PDB ID: 4UDX. **f**, Analogous use of polymeric materials to control the substrate delivery in a cobalt CO_2 reduction electrocatalyst. **g**, Structure of *Moorella thermoaceticum* CODH/ACS demonstrating the sequential catalysis and preconcentration of a second substrate. PDB ID: 1MJG. **h**, Use of a patterned bimetallic catalyst for sequential catalysis. More examples are described and referenced in the text. Panels reproduced with permission from: **b**, ref. [19], American Chemical Society; **d**, ref. [28], American Chemical Society; **f**, ref. [39] under a Creative Commons licence CC BY 4.0; **h**, ref. [62], RSC.

heterogeneous catalysts, the activity descriptors are the CO_2 and CO binding energies. However, these two properties are inversely related such that the substrate and product interaction cannot be optimized independently. Cooperative activation of CO_2 (which does not impact CO binding) breaks these scaling relationships, which enables catalytic reduction at milder potentials[21]. There are several examples of synthetic homogeneous catalysts that similarly capitalize on cooperative CO_2 activation for an enhanced reactivity or selectivity. These cooperative interactions include a secondary metal[22–24], hydrogen bonding to the anionic carboxylate oxygen[25–28] and electrostatic stabilization of the carboxylate intermediate[29–31]. An example of the third case is shown in Fig. 2d, in which phenol functionalities in the secondary coordination sphere of an iron porphyrin CO_2 to CO electrocatalyst are believed to stabilize the carboxylate intermediate through hydrogen-bonding interactions[28]. In heterogeneous systems, this cooperative interaction was mimicked through the use of bimetallic catalysts or Lewis acidic cationic additives, which are proposed to stabilize CO_2 activation intermediates[32–34]. Cationic additives can also impact the interfacial arrangement of ions at the surface of electrodes when a potential is applied[35].

Inhibiting H_2 evolution can also be influenced by the catalysts' secondary structure and microenvironment. For example, proton sources are hydrophilic (or solvated under aqueous conditions), whereas CO_2, as a relatively inert non-polar molecule, is not. Thus, modifying the hydrophilicity and/or hydrophobicity or polarity of the environment around the catalyst active site to mediate the proton flow offers another bio-inspired strategy to achieve selective reduction. Proton transfer from the solvent into the bound CO_2 molecule in the NiFe–CODH enzymes has been suggested to occur via three conserved basic histidine residues[11], which cycle between neutral and positively charged states, along with a putative water channel (Fig. 2e). This contrasts with the [NiFe] hydrogenase enzymes, which are proposed to use a combination of water molecules and primarily acidic residues for proton transfer[36], and suggests that the polarity of the distal environment is important. Support for this general phenomenon was observed through a study of CO_2 reduction activity by a synthetic catalyst, $[Ni(cyclam)]^{2+}$ (cyclam, 1,4,8,11-tetraazacyclotetradecane), across different buffers, in which a full selectivity towards CO_2 reduction over H^+ reduction was accessible in a basic buffering media[37]. The importance of the buffer as a proton donor, independent of pH, was also shown in heterogeneous[38] CO_2 electrocatalytic reductions. Polymer encapsulation provides an intermediate degree of complexity to the catalyst microenvironment and presents a random arrangement of hydrophobic and charged groups that, in the case of cobalt phthalocyanine, were shown to enhance selectivity by converting proton transfer from a bimolecular into an intramolecular process (Fig. 2f)[39]. Thus, both the proton source and microenvironment can work to control proton flow and overall product selectivity. Given that enzymes can be considered to be highly unsymmetric polymers that encapsulate a catalyst, this approach offers an opportunity for the biological and the bio-inspired worlds to meet in the middle: polymers can be synthesized with increasing complexity and asymmetry and wrapped around catalytic sites[40], whereas enzymes can be deconstructed by selective removal of auxiliary subunits or cofactors. Through these complementary tactics, the minimal functional units necessary for selective CO_2 reduction can be established.

A related approach in synthetic catalysts capitalizes on electrostatic effects to engender a greater selectivity for CO_2 reduction. Local cationic charges, introduced through the use of ionomers and other additives at heterogeneous active sites[34,41–43] or incorporated into molecular complexes[44], can result in larger overpotentials for the H_2 evolution reactions, possibly due to an inhibited access of the protons to the catalyst active sites. Although the local proton concentration and pathway to approach the catalyst is inhibited by cationic charge, the neutral CO_2 substrate is not as strongly affected.

Another proposed bio-inspired structural strategy to enhance CO_2 reduction over proton reduction is through spatial separation

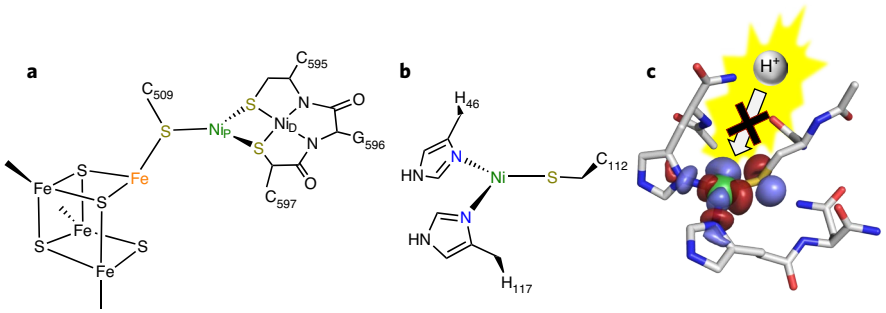

Fig. 3 | Structural and electronic elements for selective C–C bond formation. a, Active site structure of *M. thermoacetica* acetyl coenzyme A synthase (ACS). **b**, Active site structure of *P. aeruginosa* M121A nickel-substituted azurin as an ACS model. **c**, A singly occupied molecular orbital (SOMO) of Ni^{I}Az highlights the substantial contribution from the thiolate sulfur atom. The symmetry and distribution of the SOMO are orthogonal to the substrate binding channel, which precludes interaction with an incoming proton.

of the protons and electrons. This is the strategy suggested in nearly all mechanisms for the enzyme formate dehydrogenase, which formally transfers a hydride to CO_2 (two electrons and a proton). Instead of a classic metal hydride intermediate, the major mechanistic proposals state that the electrons and protons are not co-located on the metal. In these mechanisms, the Mo or W centre cycles between a +4 and a +6 oxidation state. The proton required to complete the hydride comes from a ligand or the secondary coordination sphere: from a terminal sulfido, a dissociated (seleno)cysteine ligand or an outer-sphere histidine residue, arginine residue or cysteine residue[45,46]. Formate dehydrogenase exhibits negligible parasitic H_2 evolution during CO_2 reduction in an otherwise reducing environment[47,48]. We have suggested that spatially separating the electron and proton source can lead to inhibited H_2 evolution[49]. A proton source positioned at an appropriate distance from the electron source (metal) could transfer both proton and electrons to a larger CO_2 substrate that can bridge the gap between them when a smaller proton would not be able to accept the necessary electrons and/or protons for H_2 evolution. This strategy also appears to be at play in the active site of NiFe–CODH, where electrons transfer from the metallocluster and protons likely come from the lysine residue.

Strategies for C–C bond formation

To develop architectures for sequential reactions that efficiently and selectively convert CO_2 into more complex ($C \geq 2$) value-added products and fuels, the catalyst environment must be considered across many length scales. Nature provides inspiration to develop such scaffolds, as highly selective and efficient cascade reactions are prevalent across natural enzyme systems. The CO dehydrogenase/acetyl coenzyme A synthase (CODH/ACS) enzyme complex represents one highly evolved example of such a system, and demonstrates an extensive dynamic motion to choreograph the synthesis of a new C–C bond in acetyl coenzyme A from one-carbon precursors. Identifying the structural and electronic features that underpin this unique reactivity is vital for the design of similarly effective anthropogenic catalysts.

During acyl synthesis by CODH/ACS, the CO_2-derived carbon monoxide leaves the CODH active site and enters a hydrophobic gas channel that leads to the ACS active site, called the A cluster (Fig. 3a)[11,47]. Within the A cluster, the key catalytic centre is thought to be the proximal nickel site (Ni_P), and the distal nickel ion (Ni_D) is presumed to play a structural role. Both the CO substrate and a cationic methyl group, donated by a cobalamin methyl transferase protein, bind to the Ni_P centre, which catalyses acyl formation in a process analogous to the commercial Monsanto reaction[50]. As for the CODH active site, a strong electronic communication between the Ni_P centre and the [4Fe–4S] cluster is mediated through the bridging thiolate ligand, and reactivity towards each substrate depends on the active-site redox state[51]. Acyl transfer to the coenzyme A thiol group appears to be substrate-gated, and occurs rapidly once CoA is introduced. In total, ACS catalyses the formation of both a C–C and a C–S bond.

Although synthetic inorganic compounds designed to model ACS provide a precedent for the reactivity of a low-coordinate, low-valent nickel centre with CO and methyl ligands, to date, no synthetic nickel compound has been able to reversibly catalyse the formation and catabolism of a thioester without degradation of the active site[52,53]. Protein-based models, such as those developed by Shafaat and co-workers, which were derived from a nickel-substituted mutant of *Pseudomonas aeruginosa* azurin, expand our understanding of these limitations. A Ni^{I} state is readily obtained in this nickel azurin-based model of ACS (M121A NiAz; Fig. 3b), which exhibits similar electronic properties to those of the native enzyme, indicating that two histidine imidazole ligands may mimic the electronic structure of the two bridging thiolate ligands between the nickel centres[54]. This suggests that in a synthetic model of ACS, the Ni_D subsite could be replaced with pyridine or pyrazole ligands, often used to replicate histidine ligation. The Ni^{I}Az state binds both CO and a cationic methyl group to give EPR-active Ni^{I}–CO and Ni–CH_3 species[54,55]. In both systems, the metal–thiolate interaction dominates the electronic structure and stabilizes the reduced species, to the extent that the formal Ni^{III}–CH_3 species is best described as an electronic d^9 Ni^{I} species with an inverted ligand field[56]. A similar electronic structure is implicated in native ACS. These studies highlight the importance of a strongly covalent ligand framework to distribute electron density, and so reduce the build up of formal and physical charge on the metal centre and direct reactivity towards the intended substrate[54,55].

Beyond observing key catalytic intermediates, the protein-derived ACS model offers insight into the selectivity of the native enzyme, which avoids the parasitic H_2 evolution or CO_2 reduction reactions despite operating at the thermodynamic potential for both. Although the reduced Ni centre in the NiAz model is accessible to solvent and small molecules, unproductive side reactions, such as protonation of the Ni^{I} state to form a Ni^{III}–H species, generation of H_2, protonolysis to release CH_4 and the binding and reduction of CO_2, do not occur. This diverges from what is seen in hydrogenases and other model compounds, in which a Ni^{III}–H species can form readily from Ni^{I} in the presence of protons and CO is a potent inhibitor[57,58]. The extreme selectivity of the NiAz model towards CO and methyl substrates mirrors that seen in ACS and is probably due to the strong, directed covalency of the metal–thiolate moiety. As is seen in Fig. 3c, the singly occupied molecular orbital of Ni^{I}Az is greatly delocalized onto the thiolate ligand, and the component on the metal centre lacks the appropriate structure to interact

with either a proton or CO_2 (refs. [56,59]). Methyl binding occurs via a non-canonical inverted ligand-field interaction, in which the methyl group can be considered to possess an empty p_z orbital[56]; such a configuration would be inaccessible to a proton and thus is hypothesized to prevent H_2 evolution. Establishing a similar electronic structure in a synthetic system may be important to avoid side reactions and obtain the selectivity of a natural enzyme.

Secondary sphere interactions are also implicated in controlling the substrate binding in ACS. The gas channel between the CODH and ACS active sites is lined by hydrophobic residues, thought to promote CO capture and accumulation. Captured within this secondary sphere, the entropic costs associated with gas binding are substantially reduced, and CO binding is considered to be a barrierless process. Having a molecular mechanism to capture and retain the CO substrate close to the active site is an effective preconcentration method (Fig. 2g). The use of partially hydrophobic polymer overcoatings may provide a crude model of this outer coordination sphere effect[60]. This strategy would bypass the low solubility limits of dissolved gases in aqueous solution and represents an underexplored area in catalyst design.

The idea of preconcentrating C1 substrates for subsequent C–C bond formation has been explored in heterogeneous systems, as depicted in Fig. 2h. For example, in heterogeneous catalysis, catalysts that are highly selective for CO_2 reduction to CO, such as Au or Ag, have been paired with catalysts with a higher activity towards CO reduction to higher-order hydrocarbons (that is, Cu). The spatial orientation of the catalysts is critical to improving the local concentration of CO to achieve higher concentrations of more valuable, longer-chain products[40,61,62]. Likewise, tandem or cascade catalytic systems are used in CO_2 hydrogenation to CH_3OH with molecular catalysts, with each catalyst optimized for a sequential step[63,64]. Nanoconfinement of enzymes in extended porous materials was also shown to be a highly effective strategy to reproduce cellular cascades[65], and the extension of such materials for a synthetic or heterogeneous catalyst immobilization builds from these biological principles.

Conclusions

Valorizing CO_2 to fuels and targeted chemicals is a key step towards a carbon-neutral energy economy. However, substantial obstacles remain from the standpoints of catalytic efficiency (rate and overpotential), selectivity and robustness, which have prevented a large-scale implementation. Overcoming these challenges requires a transformative approach. Nature provides a blueprint to efficiently harness CO_2 as a substrate and selectively generate specific products using metalloenzymes. As illustrated in Fig. 2, there are distinct ways in which bio-inspired strategies can be directly applied to homogeneous, heterogeneous and artificial metalloenzyme catalysts. We expect these guiding principles for selective CO_2 reduction to cross-cut through different platforms. The strategies for implementation will, of course, vary. For example, the secondary coordination sphere is tuned in artificial metalloenzymes using site-directed mutagenesis, whereas in homogeneous systems it can be modified through ligand design. In heterogeneous systems, the electrolyte and buffer has been called 'the electrochemical second coordination sphere'[66]. Thus far, this bio-inspired approach has been highly successful, and resulted in synthetic catalysts with a higher efficiency, selectivity and product control. Improved communication and critical examination of the commonalities between and across these disciplines will undoubtably accelerate catalyst development. This synergy is especially critical as there are still secrets to be discovered in natural CO_2 utilization, which will continue to inspire synthetic analogues that capitalize on these effects.

Received: 11 May 2021; Accepted: 3 September 2021;
Published online: 18 November 2021

References

1. Faunce, T. A. et al. Energy and environment policy case for a global project on artificial photosynthesis. *Energy Environ. Sci.* **6**, 695–698 (2013).
2. Lewis, N. S. & Nocera, D. G. Powering the planet: chemical challenges in solar energy utilization. *Proc. Natl Acad. Sci. USA* **103**, 15729–15735 (2006).
3. Sanz-Pérez, E. S., Murdock, C. R., Didas, S. A. & Jones, C. W. Direct capture of CO_2 from ambient air. *Chem. Rev.* **116**, 11840–11876 (2016).
4. Bushuyev, O. S. et al. What should we make with CO_2 and how can we make it? *Joule* **2**, 825–832 (2018).
5. Scott, A. A big bet on the smallest molecule. *C&EN* **99**, 16–19 (2021).
6. Cardenas, A. J. P. et al. Controlling proton delivery through catalyst structural dynamics. *Angew. Chem. Int. Ed.* **55**, 13509–13513 (2016).
7. Cunningham, D. W., Barlow, J. M., Velazquez, R. S. & Yang, J. Y. Reversible and selective CO_2 to HCO_2^- electrocatalysis near the thermodynamic potential. *Angew. Chem. Int. Ed.* **59**, 4443–4447 (2020).
8. Armstrong, D. A. et al. Standard electrode potentials involving radicals in aqueous solution: inorganic radicals (IUPAC Technical Report). *Pure Appl. Chem.* **87**, 1139–1150 (2015).
9. Ceballos, B. M. & Yang, J. Y. Directing the reactivity of metal hydrides for selective CO_2 reduction. *Proc. Natl Acad. Sci. USA* **115**, 12686–12691 (2018).
10. Barlow, J. M. & Yang, J. Y. Thermodynamic considerations for optimizing selective CO_2 reduction by molecular catalysts. *ACS Cent. Sci.* **5**, 580–588 (2019).
11. Can, M., Armstrong, F. A. & Ragsdale, S. W. Structure, function, and mechanism of the nickel metalloenzymes, CO dehydrogenase, and acetyl-CoA synthase. *Chem. Rev.* **114**, 4149–4174 (2014).
12. Hu, Z. et al. Nature of the C-cluster in Ni-containing carbon monoxide dehydrogenases. *J. Am. Chem. Soc.* **118**, 830–845 (1996).
13. Breglia, R. et al. First-principles calculations on Ni,Fe-containing carbon monoxide dehydrogenases reveal key stereoelectronic features for binding and release of CO_2 to/from the C-cluster. *Inorg. Chem.* **60**, 387–402 (2021).
14. Fesseler, J., Jeoung, J.-H. & Dobbek, H. How the $[NiFe_4S_4]$ cluster of CO dehydrogenase activates CO_2 and NCO^-. *Angew. Chem. Int. Ed.* **54**, 8560–8564 (2015).
15. Eckert, N. A., Dinescu, A., Cundari, T. R. & Holland, P. L. A T-shaped three-coordinate nickel(I) carbonyl complex and the geometric preferences of three-coordinate d^9 complexes. *Inorg. Chem.* **44**, 7702–7704 (2005).
16. Blackaby, W. J. M. et al. Mono- and dinuclear Ni(I) products formed upon bromide abstraction from the Ni(I) ring-expanded NHC complex [Ni(6-Mes)(PPh_3)Br]. *Dalton Trans.* **47**, 769–782 (2018).
17. Amara, P., Mouesca, J.-M., Volbeda, A. & Fontecilla-Camps, J. C. Carbon monoxide dehydrogenase reaction mechanism: a likely case of abnormal CO_2 insertion to a Ni–H^- bond. *Inorg. Chem.* **50**, 1868–1878 (2011).
18. Wang, V. C. C., Islam, S. T. A., Can, M., Ragsdale, S. W. & Armstrong, F. A. Investigations by protein film electrochemistry of alternative reactions of nickel-containing carbon monoxide dehydrogenase. *J. Phys. Chem. B* **119**, 13690–13697 (2015).
19. Keith, J. A., Grice, K. A., Kubiak, C. P. & Carter, E. A. Elucidation of the selectivity of proton-dependent electrocatalytic CO_2 reduction by *fac*-Re(bpy)$(CO)_3$Cl. *J. Am. Chem. Soc.* **135**, 15823–15829 (2013).
20. Majumdar, A. Bioinorganic modeling chemistry of carbon monoxide dehydrogenases: description of model complexes, current status and possible future scopes. *Dalton Trans.* **43**, 12135–12145 (2014).
21. Hansen, H. A., Varley, J. B., Peterson, A. A. & Nørskov, J. K. Understanding trends in the electrocatalytic activity of metals and enzymes for CO_2 reduction to CO. *J. Phys. Chem. Lett.* **4**, 388–392 (2013).
22. Isse, A. A., Gennaro, A., Vianello, E. & Floriani, C. Electrochemical reduction of carbon dioxide catalyzed by [CoI(salophen)Li]. *J. Mol. Catal.* **70**, 197–208 (1991).
23. Bhugun, I., Lexa, D. & Savéant, J.-M. Catalysis of the electrochemical reduction of carbon dioxide by iron(0) porphyrins. Synergistic effect of Lewis acid cations. *J. Phys. Chem.* **100**, 19981–19985 (1996).
24. Steffey, B. D., Curtis, C. J. & DuBois, D. L. Electrochemical reduction of CO_2 catalyzed by a dinuclear palladium complex containing a bridging hexaphosphine ligand: evidence for cooperativity. *Organometallics* **14**, 4937–4943 (1995).
25. Beley, M., Collin, J. P., Ruppert, R. & Sauvage, J. P. Electrocatalytic reduction of carbon dioxide by nickel cyclam^{2+} in water: study of the factors affecting the efficiency and the selectivity of the process. *J. Am. Chem. Soc.* **108**, 7461–7467 (1986).
26. Fujita, E., Creutz, C., Sutin, N. & Brunschwig, B. S. Carbon dioxide activation by cobalt macrocycles: evidence of hydrogen bonding between bound CO_2 and the macrocycle in solution. *Inorg. Chem.* **32**, 2657–2662 (1993).
27. Dey, S., Ahmed, M. E. & Dey, A. Activation of Co(I) state in a cobalt-dithiolato catalyst for selective and efficient CO_2 reduction to CO. *Inorg. Chem.* **57**, 5939–5947 (2018).

28. Costentin, C., Passard, G., Robert, M. & Savéant, J.-M. Pendant acid–base groups in molecular catalysts: H-bond promoters or proton relays? Mechanisms of the conversion of CO_2 to CO by electrogenerated iron(0) porphyrins bearing prepositioned phenol functionalities. *J. Am. Chem. Soc.* **136**, 11821–11829 (2014).
29. Azcarate, I., Costentin, C., Robert, M. & Savéant, J.-M. Through-space charge interaction substituent effects in molecular catalysis leading to the design of the most efficient catalyst of CO_2-to-CO electrochemical conversion. *J. Am. Chem. Soc.* **138**, 16639–16644 (2016).
30. Sung, S., Kumar, D., Gil-Sepulcre, M. & Nippe, M. Electrocatalytic CO_2 reduction by imidazolium-functionalized molecular catalysts. *J. Am. Chem. Soc.* **139**, 13993–13996 (2017).
31. DeLuca, E. E., Xu, Z., Lam, J. & Wolf, M. O. Improved electrocatalytic CO_2 reduction with palladium bis(NHC) pincer complexes bearing cationic side chains. *Organometallics* **34**, 1330–1343 (2019).
32. Murata, A. & Hori, Y. Product selectivity affected by cationic species in electrochemical reduction of CO_2 and CO at a Cu electrode. *Bull. Chem. Soc. Jpn* **64**, 123–127 (1991).
33. Chen, L. D., Urushihara, M., Chan, K. & Nørskov, J. K. Electric field effects in electrochemical CO_2 reduction. *ACS Catal.* **6**, 7133–7139 (2016).
34. Thorson, M. R., Siil, K. I. & Kenis, P. J. A. Effect of cations on the electrochemical conversion of CO_2 to CO. *J. Electrochem. Soc.* **160**, F69–F74 (2012).
35. Liu, M. et al. Enhanced electrocatalytic CO_2 reduction via field-induced reagent concentration. *Nature* **537**, 382–386 (2016).
36. Ogata, H., Nishikawa, K. & Lubitz, W. Hydrogens detected by subatomic resolution protein crystallography in a [NiFe] hydrogenase. *Nature* **520**, 571–574 (2015).
37. Schneider, C. R., Lewis, L. C. & Shafaat, H. S. The good, the neutral, and the positive: buffer identity impacts CO_2 reduction activity by nickel(II) cyclam. *Dalton Trans.* **48**, 15810–15821 (2019).
38. Zhang, B. A., Ozel, T., Elias, J. S., Costentin, C. & Nocera, D. G. Interplay of homogeneous reactions, mass transport, and kinetics in determining selectivity of the reduction of CO_2 on gold electrodes. *ACS Cent. Sci.* **5**, 1097–1105 (2019).
39. Liu, Y. & McCrory, C. C. L. Modulating the mechanism of electrocatalytic CO_2 reduction by cobalt phthalocyanine through polymer coordination and encapsulation. *Nat. Commun.* **10**, 1683 (2019).
40. Wadsworth, B. L., Khusnutdinova, D. & Moore, G. F. Polymeric coatings for applications in electrocatalytic and photoelectrosynthetic fuel production. *J. Mat. Chem. A* **6**, 21654–21665 (2018).
41. Sarkar, S., Maitra, A., Banerjee, S., Thoi, V. S. & Dawlaty, J. M. Electric fields at metal–surfactant interfaces: a combined vibrational spectroscopy and capacitance study. *J. Phys. Chem. B* **124**, 1311–1321 (2020).
42. Banerjee, S., Han, X. & Thoi, V. S. Modulating the electrode–electrolyte interface with cationic surfactants in carbon dioxide reduction. *ACS Catal.* **9**, 5631–5637 (2019).
43. Quan, F., Xiong, M., Jia, F. & Zhang, L. Efficient electroreduction of CO_2 on bulk silver electrode in aqueous solution via the inhibition of hydrogen evolution. *Appl. Surf. Sci.* **399**, 48–54 (2017).
44. Barlow, J. M., Ziller, J. W. & Yang, J Y. Inhibiting the hydrogen evolution reaction (HER) with proximal cations: a strategy for promoting selective electrocatalytic reduction. *ACS Catal.* **11**, 8155–8164 (2021).
45. Maia, L. B., Moura, I. & Moura, J. J. G. Molybdenum and tungsten-containing formate dehydrogenases: aiming to inspire a catalyst for carbon dioxide utilization. *Inorg. Chim. Acta* **455**, 350–363 (2017).
46. Niks, D., Duvvuru, J., Escalona, M. & Hille, R. Spectroscopic and kinetic properties of the molybdenum-containing, NAD^+-dependent formate dehydrogenase from *Ralstonia eutropha*. *J. Biol. Chem.* **291**, 1162–1174 (2016).
47. Appel, A. M. et al. Frontiers, opportunities, and challenges in biochemical and chemical catalysis of CO_2 fixation. *Chem. Rev.* **113**, 6621–6658 (2013).
48. Bassegoda, A., Madden, C., Wakerley, D. W., Reisner, E. & Hirst, J. Reversible interconversion of CO_2 and formate by a molybdenum-containing formate dehydrogenase. *J. Am. Chem. Soc.* **136**, 15473–15476 (2014).
49. Yang, J. Y., Kerr, T. A., Wang, X. S. & Barlow, J. M. Reducing CO_2 to HCO_2^- at mild potentials: lessons from formate dehydrogenase. *J. Am. Chem. Soc.* **142**, 19438–19445 (2020).
50. Forster, D. On the mechanism of a rhodium-complex-catalyzed carbonylation of methanol to acetic acid. *J. Am. Chem. Soc.* **98**, 846–848 (1976).
51. Gencic, S. & Grahame, D. A. Two separate one-electron steps in the reductive activation of the A cluster in subunit β of the ACDS complex in *Methanosarcina thermophila*. *Biochemistry* **47**, 5544–5555 (2008).
52. Dougherty, W. G., Rangan, K., O'Hagan, M. J., Yap, G. P. A. & Riordan, C. G. Binuclear complexes containing a methylnickel moiety: relevance to organonickel intermediates in acetyl coenzyme A synthase catalysis. *J. Am. Chem. Soc.* **130**, 13510–13511 (2008).
53. Matsumoto, T., Ito, M., Kotera, M. & Tatsumi, K. A dinuclear nickel complex modeling of the $Ni_d(II)$–$Ni_p(I)$ state of the active site of acetyl CoA synthase. *Dalton Trans.* **39**, 2995–2997 (2010).
54. Manesis, A. C. et al. A biochemical nickel(I) state supports nucleophilic alkyl addition: a roadmap for methyl reactivity in acetyl coenzyme A synthase. *Inorg. Chem.* **58**, 8969–8982 (2019).
55. Manesis, A. C., O'Connor, M. J., Schneider, C. R. & Shafaat, H. S. Multielectron chemistry within a model nickel metalloprotein: mechanistic implications for acetyl-CoA synthase. *J. Am. Chem. Soc.* **139**, 10328–10338 (2017).
56. Kisgeropoulos, E. C., Manesis, A. C. & Shafaat, H. S. Ligand field inversion as a mechanism to gate bioorganometallic reactivity: investigating a biochemical model of acetyl CoA synthase using spectroscopy and computation. *J. Am. Chem. Soc.* **143**, 849–867 (2021).
57. Kampa, M., Pandelia, M.-E., Lubitz, W., van Gastel, M. & Neese, F. A metal–metal bond in the light-induced state of [NiFe] hydrogenases with relevance to hydrogen evolution. *J. Am. Chem. Soc.* **135**, 3915–3925 (2013).
58. Huynh, M. T., Schilter, D., Hammes-Schiffer, S. & Rauchfuss, T. B. Protonation of nickel–iron hydrogenase models proceeds after isomerization at nickel. *J. Am. Chem. Soc.* **136**, 12385–12395 (2014).
59. Manesis, A. C. & Shafaat, H. S. Electrochemical, spectroscopic, and density functional theory characterization of redox activity in nickel-substituted azurin: a model for acetyl-CoA synthase. *Inorg. Chem.* **54**, 7959–7967 (2015).
60. Xing, Z., Hu, X. & Feng, X. Tuning the microenvironment in gas-diffusion electrodes enables high-rate CO_2 electrolysis to formate. *ACS Energy Lett.* **6**, 1694–1702 (2021).
61. Morales-Guio, C. G. et al. Improved CO_2 reduction activity towards C_{2+} alcohols on a tandem gold on copper electrocatalyst. *Nat. Catal.* **1**, 764–771 (2018).
62. Lum, Y. & Ager, J. W. Sequential catalysis controls selectivity in electrochemical CO_2 reduction on Cu. *Energy Environ. Sci.* **11**, 2935–2944 (2018).
63. Huff, C. A. & Sanford, M. S. Cascade catalysis for the homogeneous hydrogenation of CO_2 to methanol. *J. Am. Chem. Soc.* **133**, 18122–18125 (2011).
64. Chu, W.-Y., Culakova, Z., Wang, B. T. & Goldberg, K. I. Acid-assisted hydrogenation of CO_2 to methanol in a homogeneous catalytic cascade system. *ACS Catal.* **9**, 9317–9326 (2019).
65. Megarity, C. F. et al. Electrocatalytic volleyball: rapid nanoconfined nicotinamide cycling for organic synthesis in electrode pores. *Angew. Chem. Int. Ed.* **58**, 4948–4952 (2019).
66. Marcandalli, G., Villalba, M. & Koper, M. T. M. The importance of acid–base equilibria in bicarbonate electrolytes for CO_2 electrochemical reduction and CO reoxidation studied on Au(*hkl*) electrodes. *Langmuir* **37**, 5707–5716 (2021).

Acknowledgements

H.S.S. acknowledges the US Department of Energy, award DE-SC0018020, for supporting research that informed this perspective. J.Y.Y. acknowledges the US Department of Energy, award DE-SC0020275, and the National Science Foundation, award CHE-2102589, for supporting research that informed this Perspective.

Competing interests

The authors declare no competing interests.

Additional information

Correspondence should be addressed to Hannah S. Shafaat or Jenny Y. Yang.

Peer review information *Nature Catalysis* thanks the anonymous reviewers for their contribution to the peer review of this work.